

Supplementary Information Inventory

Six supplementary figures, two supplementary tables.

Figure S1. Assessment of WH2 binding to DVD actin by isothermal titration calorimetry. Related to Figure 1.

Table S1. Data collection and refinement statistics. Related to Figure 2.

Figure S2. Additional views of the crystal structure. Related to Figure 2.

Figure S3. Alignments of the free and complexed VCD arms, and alignments of the free and complexed VCD bases. Related to Figure 3.

Figure S4. Actin-actin contacts in the VCD-actin structure compared to those in actin filament models. Related to Figure 4.

Table S2. Actin polymerization activity of VopL mutants. Related to Figure 5.

Figure S5. Details of the actin-side-of-arm contacts, and an additional contact between VCD chain B and actin 1. Related to Figure 5.

Figure S6. Representative pyrene actin polymerization data from the VCD mutant heterodimer experiment and thermal stability of VCD heterodimer mutants. Related to Figure 6.

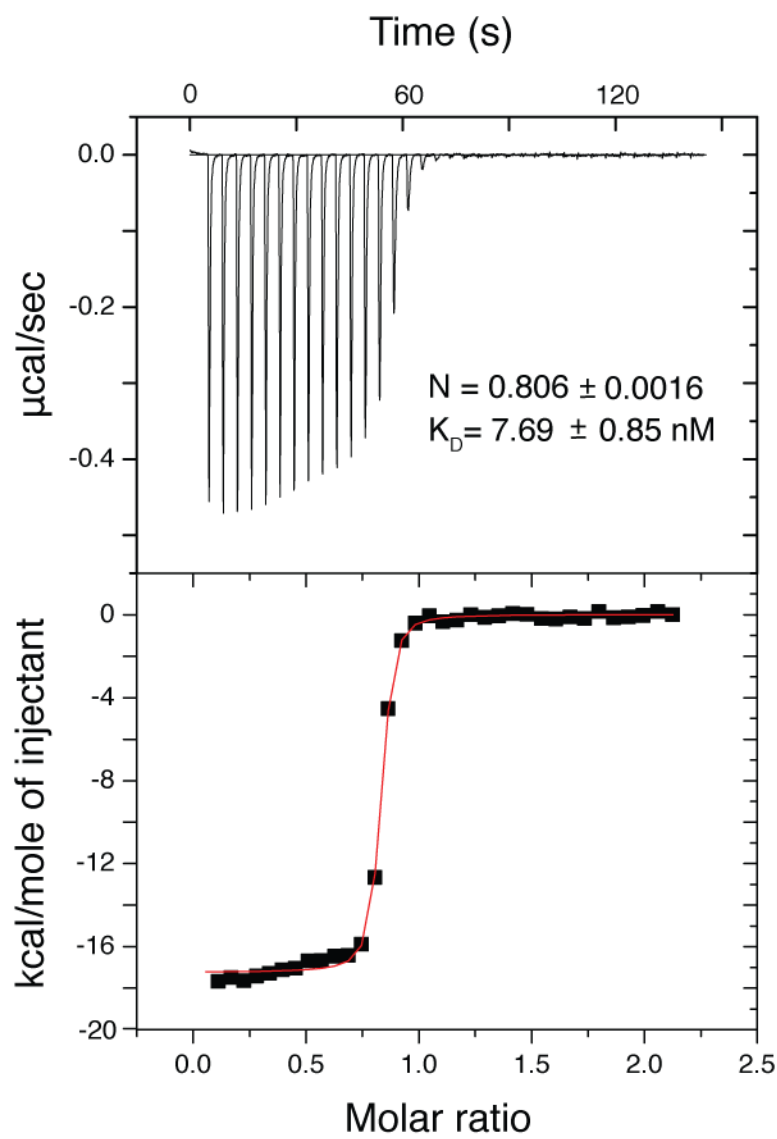


Figure S1. Assessment of WH2 binding to DVD actin by isothermal titration calorimetry. Related to Figure 1. Titration performed in KMEI buffer supplemented with 0.2 mM ATP. Upper and lower panels show raw and integrated heats, respectively. Red line in the lower panel represents the best fit to a one-site binding model. The resulting stoichiometry and K_D values appear in the top panel. The departure in the stoichiometry from the expected value of 1 is likely due to uncertainty in the concentration of the WH2 peptide.

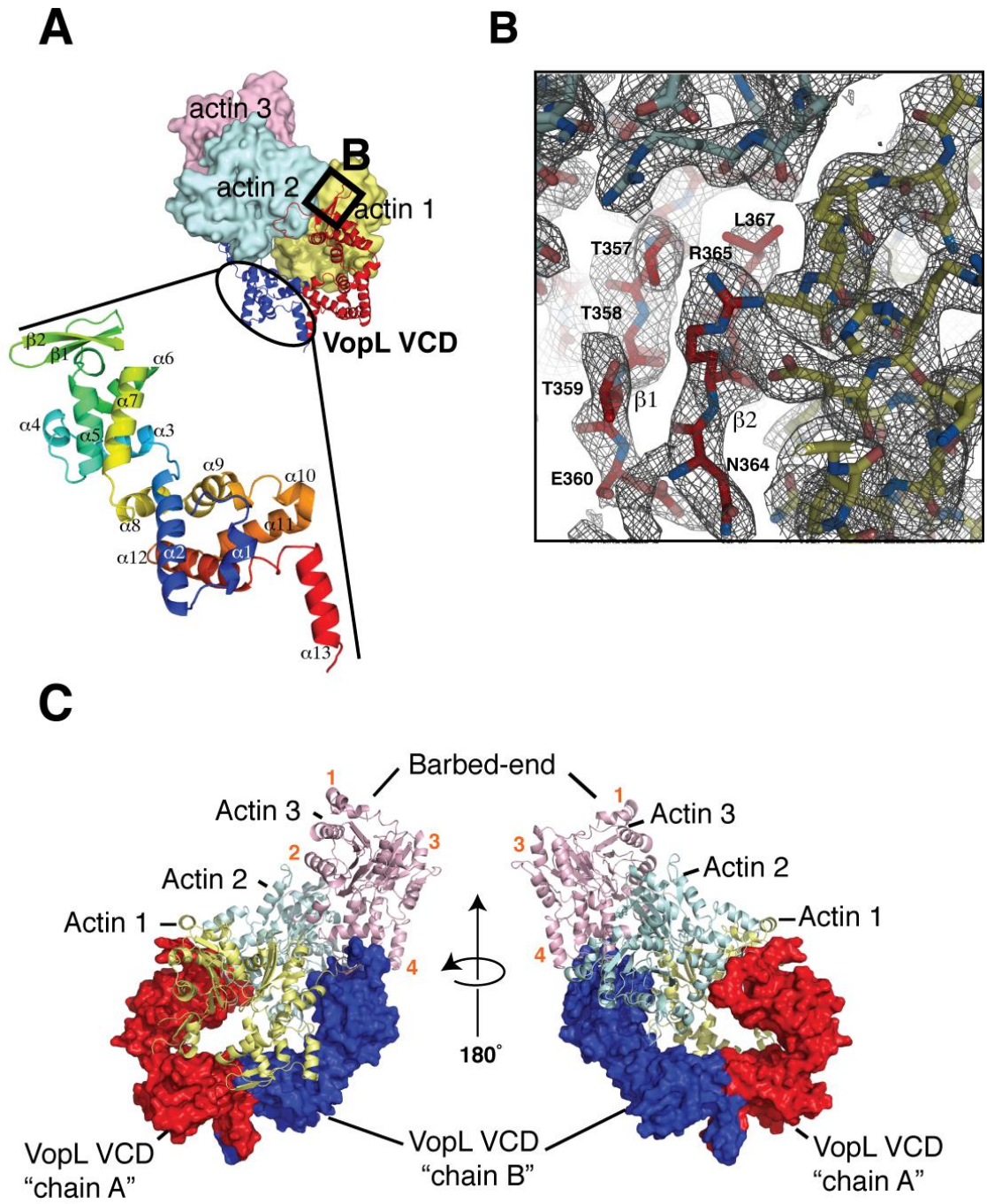


Figure S2. Additional views of the crystal structure. Related to Figure 2.

(A) Overall structure of the VCD-actin complex colored as in Figure 2. Expanded region shows a single VopL VCD monomer labeled with secondary structure elements. α -helices and β -strands are labeled in order of appearance proceeding from the N-terminus to the C-terminus. In the magnification, the VCD backbone is colored with N-terminal residues in blue, C-terminal residues in red and intermediate residues spanning the rainbow according to sequence position.

(B) Representative example of 2Fo-Fc electron density contoured at 1σ and the refined model, in the region inside the box drawn in panel A. In this region, the VCD chain A $\beta 1$ - $\beta 2$ hairpin interacts with actins 1 and 2, forming side contacts with the former, and tip contacts with the latter. The colors of carbon atoms of VCD chain A, chain B, actin 1, and actin 2 correspond to the colors of the corresponding representations depicted in panel A. Nitrogen and oxygen atoms are colored red and blue, respectively. VopL secondary structure elements and residues are labeled.

(C) Alternative view of the VCD-actin complex depicting VopL in surface representation and actin in ribbon representation. VopL monomers within a dimer appear as surfaces colored either blue or red. Actin monomers appear in ribbon representation and are colored yellow, cyan, or pink. The VopL chain identities and the identities of the actin monomers are indicated. The location of the apparent actin barbed end is indicated and actin subdomains 1-4 are indicated by orange numbers.

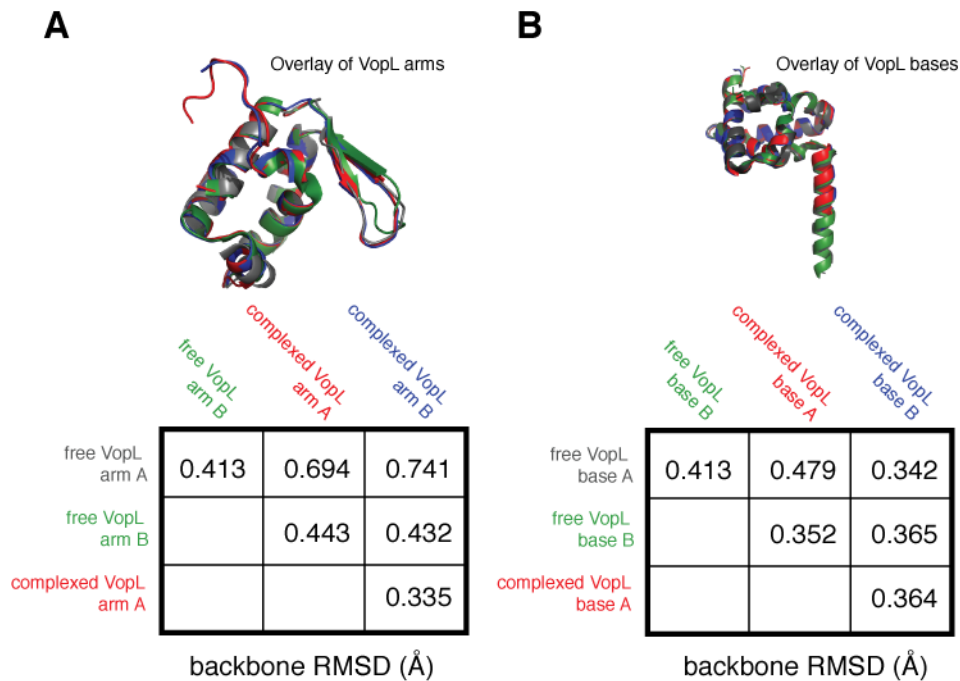


Figure S3. Alignments of the free and complexed VCD arms, and alignments of the free and complexed VCD bases. Related to Figure 3.

(A) Alignments of the free and complexed VopL arms. The table indicates the RMSD values for all possible pairwise backbone alignments of the of the four VopL arms. The alignment was restricted to residues 283-322, 340-355, and 369-382, which are ordered in both arms in both structures.

(B) Alignments of the free and complexed VopL bases The table indicates the RMSD values of all possible backbone alignments of the four VopL base subunits. The entire VopL base was used in the alignments.

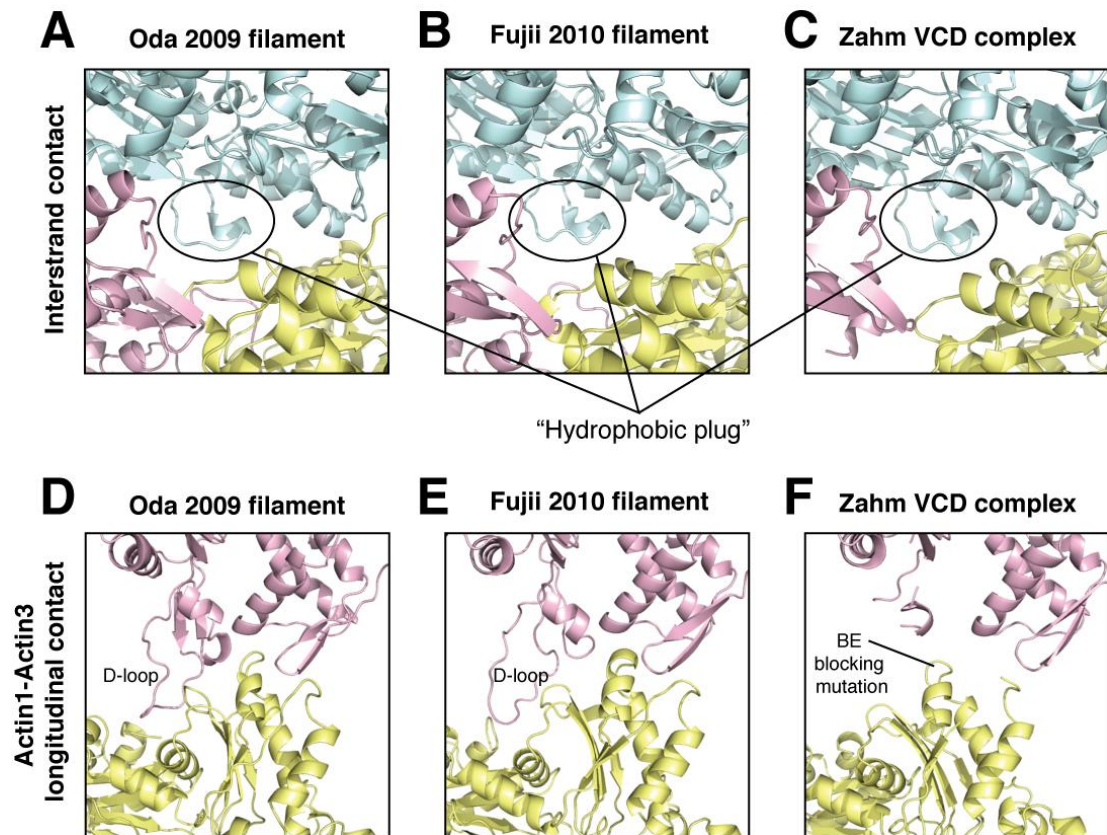


Figure S4. Actin-actin contacts in the VCD-actin structure compared to those in actin filament models. Related to Figure 4. Comparison of selected actin-actin contacts in three actin models: (A and D) a filament model derived from oriented fiber diffraction (Oda et al). (B and E) a filament model derived from cryo-electron microscopy (Fuji et al.). (C and F) The VopL-actin complex presented in this paper. Panels A, B, and C, show the organization of actins at the interstrand interface, highlighting the 'hydrophobic plug.' This element contacts the opposing paired strand at the longitudinal interface between two actins. In the three models, this loop occupies a similar location. Panels D, E, and F, show the longitudinal actin-actin contact made in the three models. Filament models are characterized by the ordering of the D-loop and its insertion into a cleft in the opposing actin. In the VopL complex, the D loop is not ordered or inserted into the yellow (lower) actin cleft, and the yellow actin has been rotated away from the proper orientation by several degrees. This interface includes the DVD mutations blocking the filament barbed end.

VopL Construct	$t_{1/2}$ (s) at 50 nM
Actin control	1352 +/- 51
Wild type	41 +/- 10
Arm mutants	
K323E / R347E / R354E	300 +/- 12
D326G / V327G / P333G	132 +/- 6
Base mutants	
K421A / Y425A / R428D	112 +/- 17
Y425A / R428D	98 +/- 5
E408K / D413K / E417A	64 +/- 6

Table S2. Actin polymerization activity of VopL mutants. Related to Figure. 5.

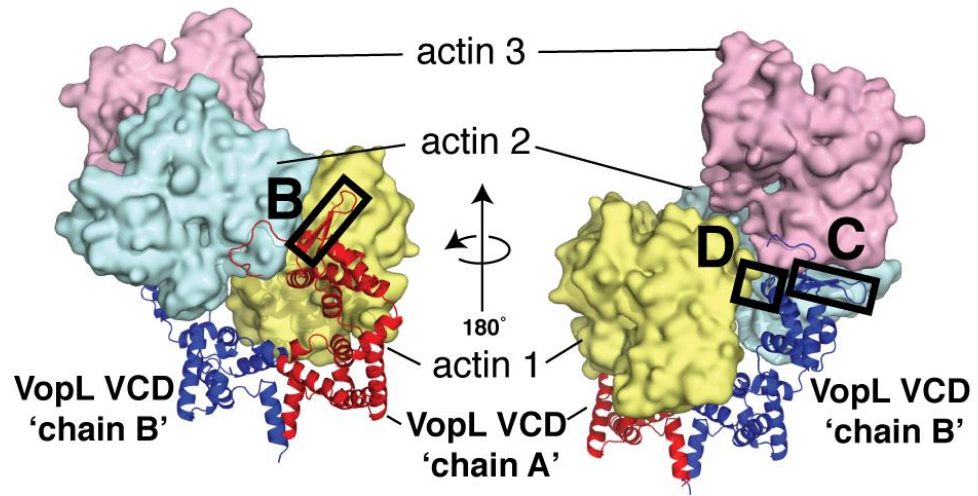
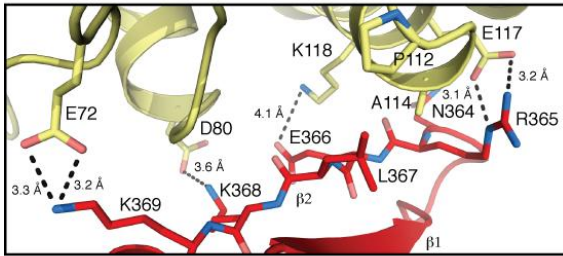
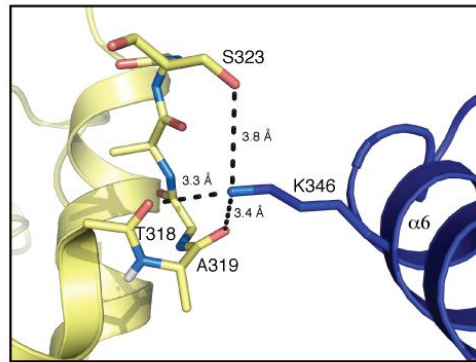
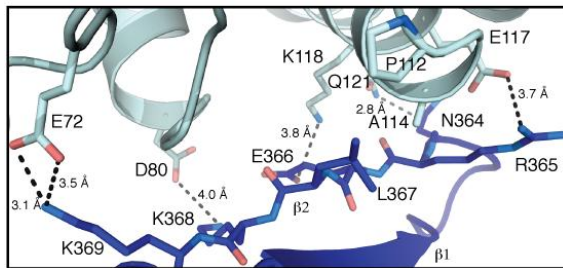
A**B****D****C**

Figure S5. Details of the actin-side-of-arm contacts, and an additional contact between VCD chain B and actin 1. Related to Figure 5.

In all panels coloring and representations match those in Figure 5. Residue numbers and secondary structural elements are indicated. Contacts within 4 Å are shown as dotted lines. Probable hydrogen bonds have distances indicated.

(A) Entire VCD-actin complex. The VopL chain identities, and the actins numbers are labeled. Boxes indicate the specific regions that appear in the close-up views in panels B and C.

(B) Interface between VCD chain A arm and actin 1.

(C) Interface between VCD chain B arm and actin 2.

(D) Interface between VopL chain B arm and actin1.

The details of the side-of-arm contacts between the VCD chain A arm and actin 1 are analogous to those involving the VCD chain B arm and actin 2. The interfaces are predominately electrostatic and polar in nature, with actin residues Q121, E117, K118, D80 and E72 in subdomain 2 forming contacts with VopL residues in the second β -strand: N364, R365, E366, K368 and K369, respectively (B and C). An additional small hydrophobic patch is composed of actin residues P112 and A114 in subdomain 2, and VopL residue L367, also in the second strand.

(D) Depicts an interaction between VCD chain B and actin 1 that has no analogous counterpart in VCD chain A (Fig. S9). This is a polar interaction between K346 in the $\alpha 6$ helix of VCD chain B and the backbones of T318 and A319 of actin 1, as well as with the side chain of actin residue S323.

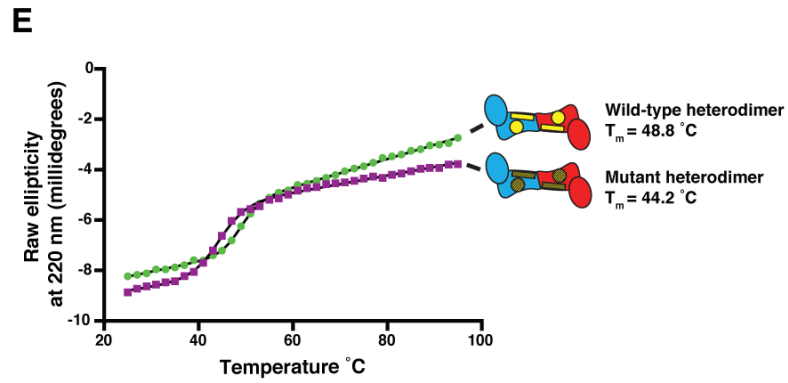
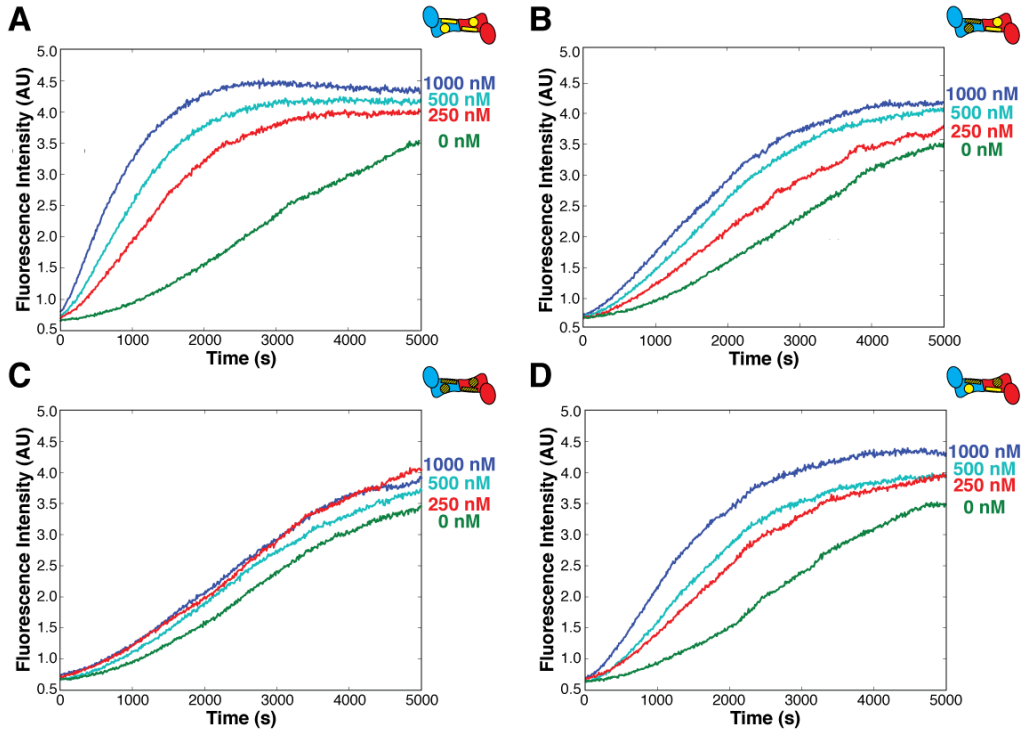


Figure S6. Representative pyrene actin polymerization data from the VCD mutant heterodimer experiment and thermal stability of VCD heterodimer mutants. Related to Figure 6.

(A-D) representative pyrene actin polymerization experiments, at 2 μM actin, 10% pyrene labeled, in KMEI, at the indicated VopL VCD concentrations. Panels differ only in the identity of the heterodimer added.

(A) Wild type heterodimer

(B) Heterodimer with both base patches mutated in the one subunit

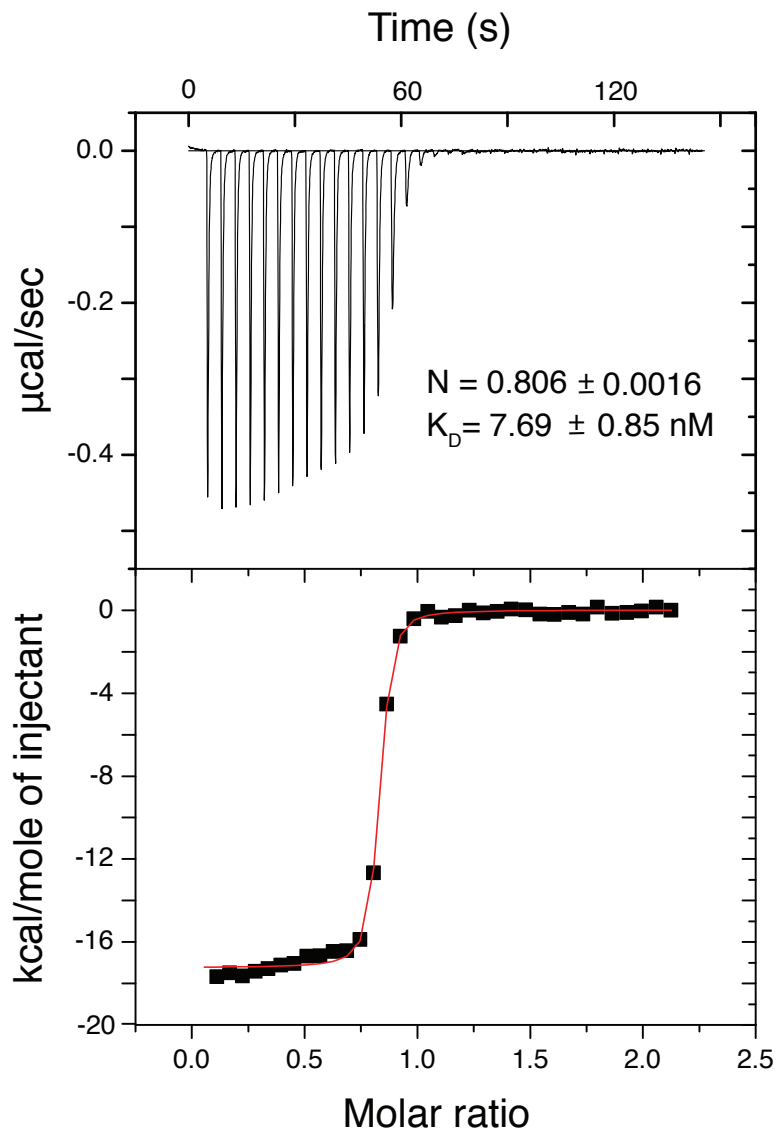
(C) Heterodimer with both patches mutated in both subunits.

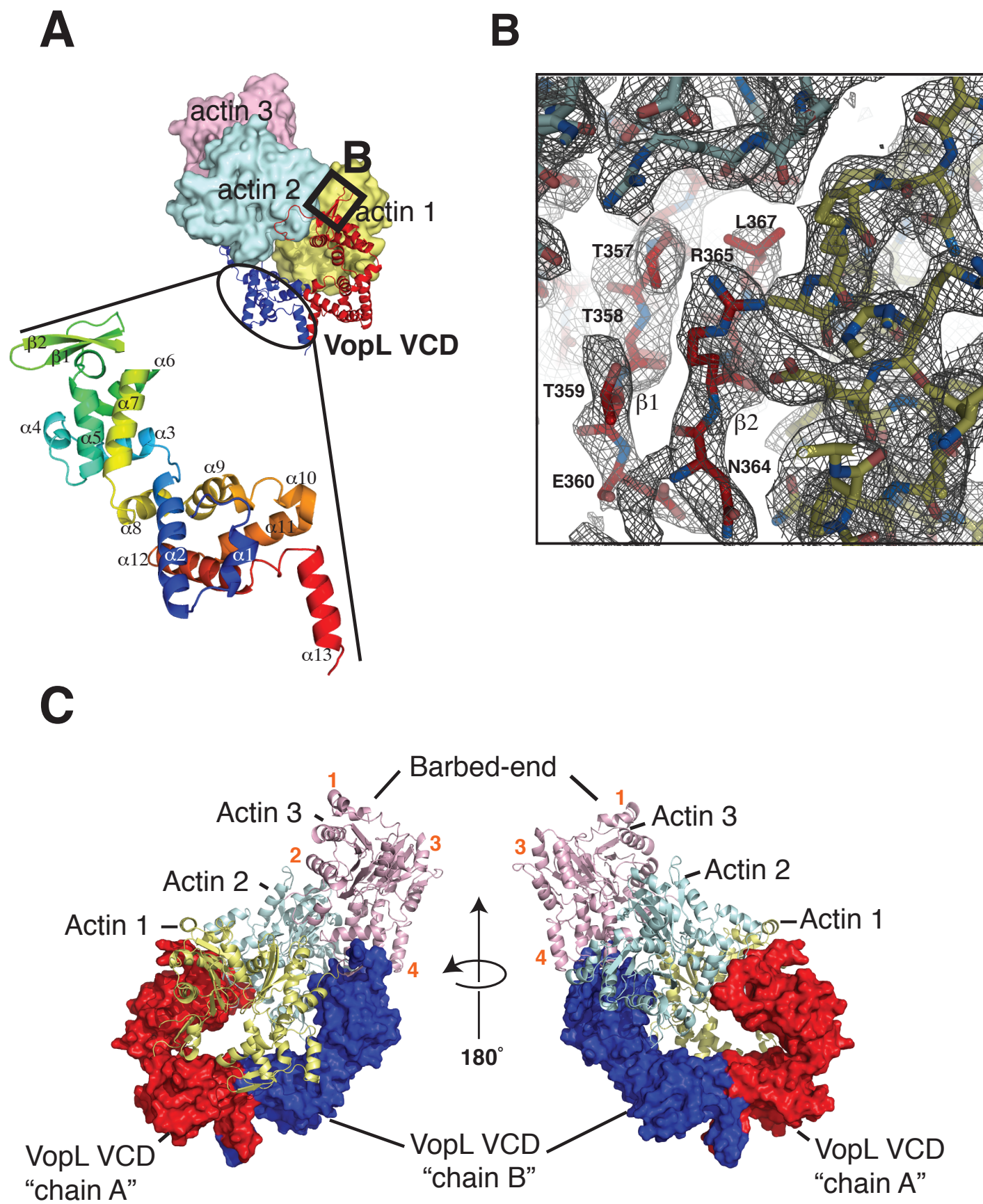
(D) Heterodimer with one patch mutated in one subunit, and the other patch mutated in the other subunit.

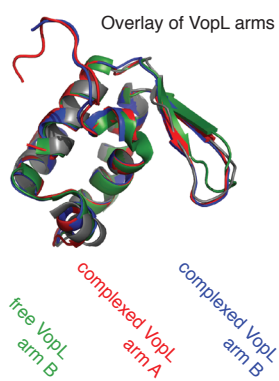
(E) Mutant VopL heterodimers exhibit comparable stability to that of wild-type heterodimers. The plot shows raw ellipticity at 220 nm of 0.1 mg/mL samples, as a function of temperature. The data for the wild-type and mutant heterodimers are shown as green circles and purple squares, respectively. The lines represent the best fit to a six-parameter sigmoidal function. Schematic representations of the heterodimers tested, along with their associated T_m values appear to the right of the graph.

Supplemental References:

Karplus, P.A., and Diederichs, K. Linking crystallographic model and data quality. *Science* 336, 1030-1033.

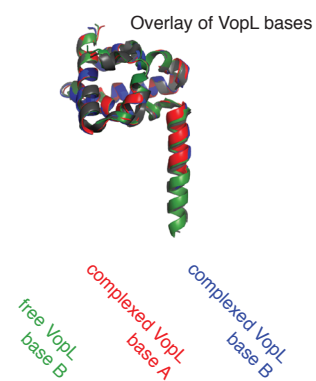




A

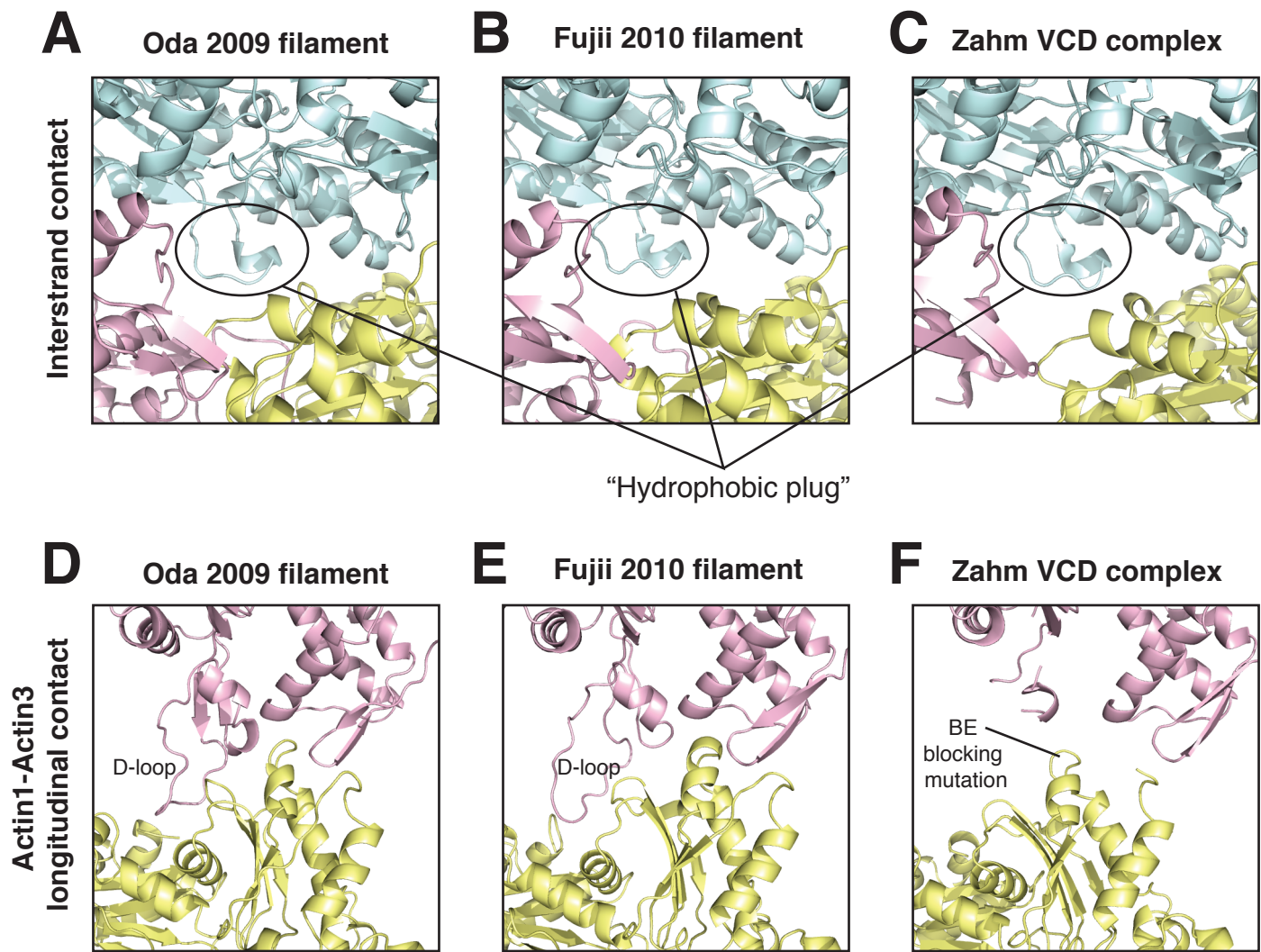
free VopL arm A	0.413	0.694	0.741
free VopL arm B		0.443	0.432
complexed VopL arm A			0.335

backbone RMSD (Å)

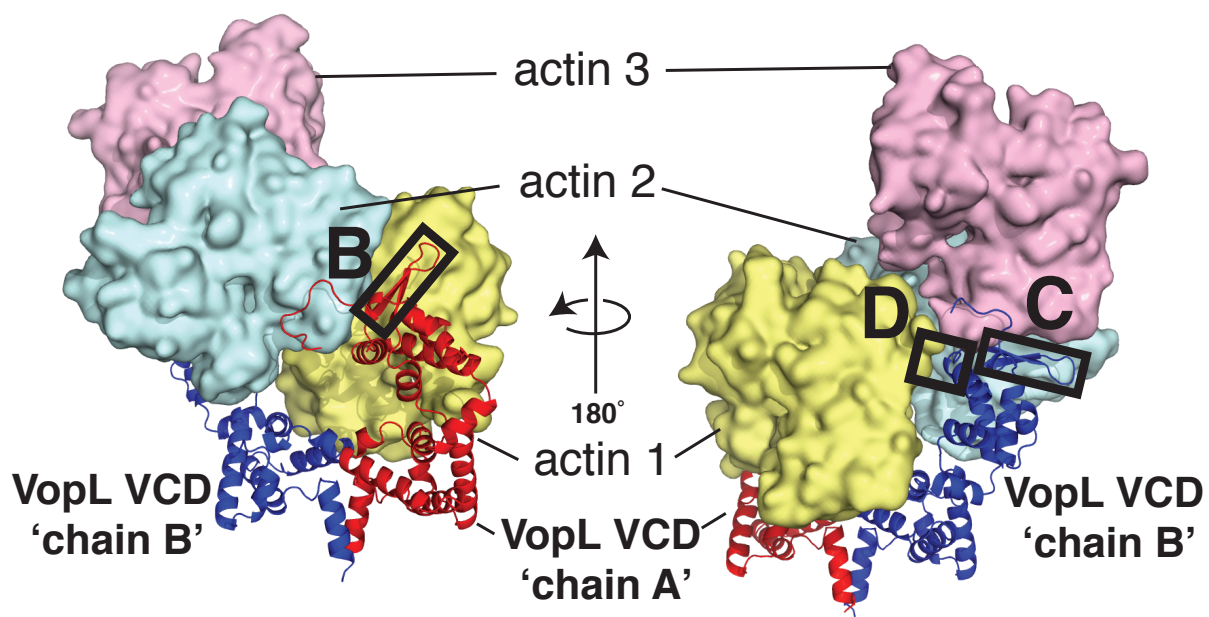
B

free VopL base A	0.413	0.479	0.342
free VopL base B		0.352	0.365
complexed VopL base A			0.364

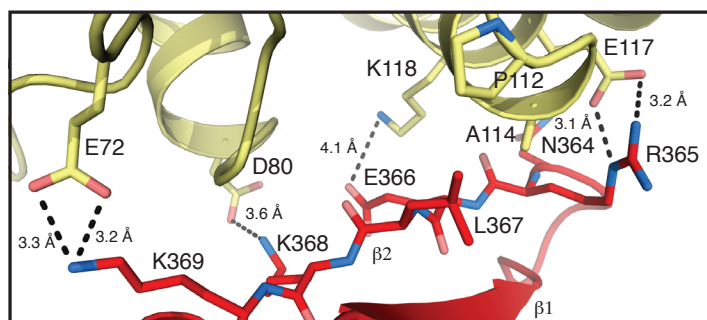
backbone RMSD (Å)



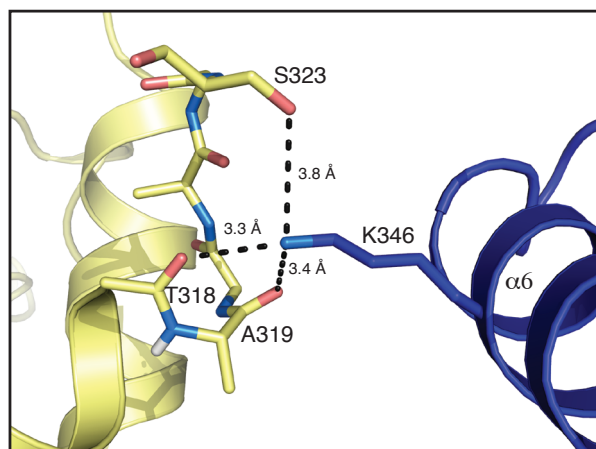
A



B



D



C

